Bio-Design and Manufacturing (2021) 4:22–32
https://doi.org/10.1007/s42242-020-00101-8

RESEARCH ARTICLE

3D kinematic mandible model to design mandibular advancement devices for the treatment of obstructive sleep apnea

M. García[1] · J. A. Cabrera[1] · A. Bataller[1] · S. Postigo[1] · J. J. Castillo[1]

Received: 28 July 2020 / Accepted: 6 October 2020 / Published online: 5 November 2020

Abstract

Mandibular advancement devices (MADs) are one of the treatments used for Obstructive sleep apnea (OSA). MADs try to maintain the mandible in an advanced position to keep the upper airways open when sleeping. To achieve this goal, most current MADs limit the mouth opening to a few millimetres. The study of the kinematic behaviour of the patient's jaw is essential in order to design devices that allow greater aperture ranges. For this purpose, a 3D multibody model that reproduces jaw movement has been developed in this work. To this end, the movement of the lower incisor has been determined by means of a vision system and reflective markers. In addition, the kinematics of the temporomandibular joint has been modelled. Next, the device is designed and printed using a cam–follower mechanism. This way, the cam profiles and the followers are optimally designed and positioned for each patient depending on the physiognomy of the jaw and the opening and advancing movement prescribed by the specialist.

Keywords Mandibular advancement device · 3D mandible kinematics · Cam–follower mechanism · 3D printed devices

Introduction

Sleep apnea is a serious disorder in which patients stop breathing for short periods of time when they are asleep [1, 2]. This disorder leads to fatigue and sleepiness during the day and it is also associated to a higher risk of developing cardiovascular problems such as arrhythmias, strokes and heart attacks [3–5].

The most common type of sleep apnea is the obstructive sleep apnea (OSA). OSA is a chronic disease in which the upper airway is repeatedly, partially or completely obstructed while sleeping. This disorder requires treatment in order to alleviate its effects [6]. The main existing treatments are continuous positive air pressure (CPAP), Oral Appliances (OA) and surgery. CPAP is a machine connected to the patient while sleeping that maintains a positive air pressure in the upper airways by means of a face mask. The main problems reported by patients are related to the noise produced by the machine and the excessive dryness of the upper airways. In those cases presenting mild to moderate OSA, an alternative to CPAP are the Mandibular Advancement Devices (MADs), which are a type of OA [7]. MADs are designed to keep the mandible in an advanced position so that the upper airway is open and does not collapse when the patient sleeps [2, 8, 9]. These devices are composed of two pieces that fit into the dental arches and force the jaw to remain in a protruded position [10, 11]. Compared to CPAP, MADs are not noisy and they are much more economical, easy to use and do not require a power system.

There is currently a wide variety of MAD models, with different strategies to keep the jaw in an advanced position [12]. Several methods are used to connect the two pieces that compose a MAD. These methods include the use of bars, elastic straps, springs, telescopic rods, tube connectors and lateral fins among others [13]. The use of this type of mechanism reduces the degrees of freedom of the jaw and limits mouth opening and lateral motion. However, users prefer models that allow wider ranges of mouth opening and lateral movement of the jaw [7]. Other valued features are maximum space for the tongue and no metallic parts. In this sense, devices using lateral fins or cams are a feasible solution that fulfils

Electronic supplementary material The online version of this article (https://doi.org/10.1007/s42242-020-00101-8) contains supplementary material, which is available to authorized users.

✉ J. A. Cabrera
jcabrera@uma.es

[1] Department of Mechanical Engineering, University of Málaga, C/ Doctor Ortiz Ramos s/n, Ampliación Campus Teatinos, 29071 Málaga, Spain

the previous demands. On one hand, there are no moving elements, such as bars or springs and, on the other hand, there are no metal parts in contact with the tongue. In addition, devices based on the use of cams can be designed to allow lateral movement of the jaw. All these devices do not take into account the kinematics of the patient's mandible. Therefore, the movement of the jaw when the device is used is not known a priori and may cause the device to lose effectiveness when the patient opens the mouth.

For this reason, the study of the patient's jaw movement is required to design customized devices. This way, some research works related to the kinematic and dynamic behaviour of the jaw have been conducted [14, 15]. These works focus on the behaviour of the jaw in mastication processes. Similarly, several robots that try to imitate jaw movements in chewing have been studied [16–19]. These results are used to propose rehabilitation methods and to study the behaviour of muscles and forces involved in mastication processes.

Biomimetic engineering can be used for the development of these robots and mechanisms. This way, the movement of the jaw is studied and recorded. Next, these devices are designed to reproduce this movement as faithfully as possible. Related to this, there are works that measure the movements of the mandible. One of the first researchers to study the jaw kinematics was Posselt, where the border movements in the sagittal, frontal and lateral planes of the lower incisor were described [20]. Many research groups have tried to reproduce these diagrams using devices mounted on the dental arches [21–24]. These works have contributed to achieving a better knowledge of the movements of the jaw and, thus, a more accurate determination of its border movements. The study of mandible motion can be used to detect problems in the temporomandibular joint and establish movement patterns that help to design robots and mechanisms, among other applications.

To the best of our knowledge, only one paper has been devoted to describing a method to design personalized devices based on the use of lateral fins or cams depending on the patient's jaw kinematic [25]. Not taking into account the movement of patient's jaw can cause MADs to be ineffective when opening the mouth and poor performance which may cause the patient to drop out of treatment.

In a previous work developed by this research group, a kinematic model of the jaw with two degrees of freedom was described [25]. However, only the movement in the sagittal plane was considered. This methodology yields to a symmetrical design of the cams in the MAD. As a result, the left side cam profile was exactly the same as the right side one and both cams were in the same relative position. While the proposed methodology in the cited work performed properly in most patients, it may cause the device to malfunction in patients with temporomandibular joint asymmetry and malformations. To cope with this lacks, this work has been developed to improve the design of MADs, allowing their personalization by means of a 3D kinematic model that reproduces the movement of patients' mandibles considering the two temporomandibular joints separately and their possible asymmetry.

Therefore, the aim of this study is to obtain an accurate kinematic model of the mandible and temporomandibular joint of a patient. To achieve this goal, a system that records jaw movements in 3D by means of infrared cameras and markers at different points of the mandible has been used. Once the model of the jaw has been obtained, the design of the mandibular advancement device can be carried out. The proposed MAD is composed of two different parts. The lower part consists of a splint with two cams, one on each side of the splint. This lower splint is designed to be joined to the mandible. Similarly, the upper part is a splint with two followers, one on each side, which is positioned in the maxilla. The followers have a semicircular profile. They contact the cams with their front side. This way, the movement of the followers, and therefore of the jaw, are determined by the profiles of the cams. The final design guarantees that the mandible does not move backwards at any time while opening the mouth. The design also takes into account factors that help to improve the comfort level such as high lateral movement, free tongue space, non-metallic pieces and non-intrusive cam design.

Therefore, the main contributions of this paper are the following:

- To develop a 3D kinematic model of the mandibular movement.
- To detail the methodology to accurately measure the movement of the mandible using a new camera/vision-based measurement system.
- To describe the methodology to design customized mandibular advancement devices for patients with asymmetries in the jaw movement.
- To apply this new approach to a real case and compare the results obtained with a previously proposed method.

This paper has been structured as follows. In "Three-dimensional mandibular movement recording system" section, the three-dimensional system used to record jaw motion is described. Once the movement of the lower incisor has been determined, the procedure to obtain the kinematics of the temporomandibular joint is developed in "Mathematical model to obtain condyle trajectories" section. Then, in "Design of a mandibular advancement device" section, natural coordinates are used to create a 3D multibody model of the mandible based on previous results. The methodology to design the mandibular advancement device personalized for each patient is also included in this section. Finally, the

Fig. 1 **a** Vicom infrared camera system. **b** Trihedrons with markers to record mandible movements

conclusions of this work are drawn in "Final considerations" section.

Three-dimensional mandibular movement recording system

Accurate measurement of the patient's jaw movement is required to properly design customized devices. In a previous work, a patient's scanner or X-Ray was used to measure the mandibular length, the condyle radius and the *x*–*y* coordinates of the maximum and minimum points of the articular fossa curve [25]. The rest of the needed values, such as protrusion (Pr), retrusion (Re) and mouth opening (MO), could be measured by an orthodontist or a dentist. It has been observed that this methodology is not adequate for patients with asymmetries in the jaw movement. In these cases, it is required to determine the movement of the trajectories of both condyles. This way, a 3D Vicon system (Oxford Metrics®, Oxford, UK) with four infrared cameras was used to determine the jaw movement in this paper. To this end, two trihedrons with six markers were manufactured and inserted between the lower and upper dental arches of a patient with a splint (see Fig. 1).

The design of the trihedrons was carried out using Solidworks®. The design was transferred to a Stratasys® 3D printer, model Objet350 Connex3™. The material used to manufacture the trihedrons was VeroDentTM. This material was selected due to its strength and durability. The combination of a 3D printing accuracy of up to 200 microns and the use of the aforementioned material allows high-quality details and an accurate manufacturing process.

The movement of the upper and lower incisor and, consequently, the border movement of the lower incisor can be obtained with this system. To do so, the specialist indicates the required movements to the patient to determine the limits of mouth opening and protrusion, retrusion and lateral movement of the mandible. All these movements are recorded by the system at a frequency of 100 Hz and subsequently processed to obtain the model of the mandibular movement. The jaw model and the markers that have been used to determine the positions of the upper and lower incisor and the right and left condyle are shown in Fig. 2.

It has to be noted that protrusion decreases with the opening of the mouth [26]. Therefore, there is a slight influence on the maximum protrusion value due to the thickness of the splint. However, the final manufactured mandibular advancement device has the same splint thickness as the trihedron splint. This way, the protrusion caused during the measurement process is the same as the one generated when the patient uses the device.

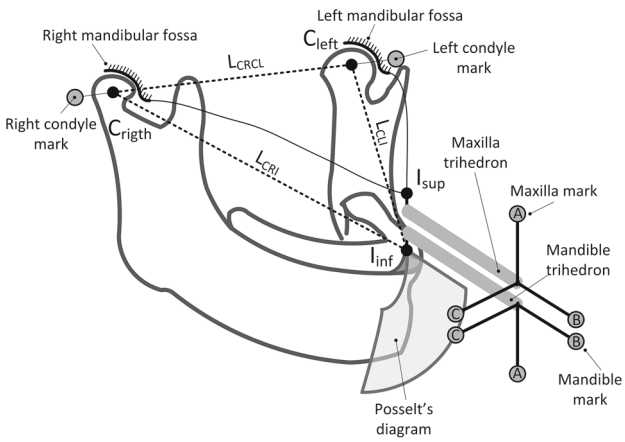

Fig. 2 3D model of the jaw with markers to determine incisor and condyle movements

Mathematical model to obtain condyle trajectories

A 3D mathematical model is required to determine the trajectories of both condyles. The use of a 2D model cannot accurately reproduce the trajectory of both condyles in case of patients with malfunctions of the jaw. This way, this section is devoted to describing a procedure to obtain the movement of the incisors and condyles using a 3D model. First, the position of two reference points on the lower and upper incisor (I_{sup} and I_{inf}) are obtained from the coordinates of each of the trihedron marks (A, B and C) during the prescribed movements (see Fig. 3).

Once the positions of each of the trihedron marks of the mandible and maxilla have been measured, the position of the lower and upper incisor can be obtained at each instant. In addition, the rest position of the right and left condyle can also be obtained. To do so, two markers are placed on the outer part of each condyle. Knowing the position of the condyle with respect to the mark, the distance between the two condyles (L_{CRCL}) and the distances from them to the reference point of the lower incisor (L_{CRI} and L_{CLI}) are determined by conducting a stationary test in the resting position of the jaw. The accuracy of these values depends on the correct positioning of the condyle mark.

These distances can also be measured on an X-ray or scan of the patient. This way, the positions of the lower incisor and right and left condyle with respect to a reference system fixed to the upper incisor are obtained (see Fig. 4). This method allows a direct and accurate measurement of L_{CRCL}, L_{CRI} and L_{CLI} lengths. However, the main disadvantage is that the patient needs to be X-rayed.

The first step is to obtain the position of the origin of the coordinate system defined by the lower and upper trihedrons, O_I and O_S, respectively. To this end, the following system of equations has been used:

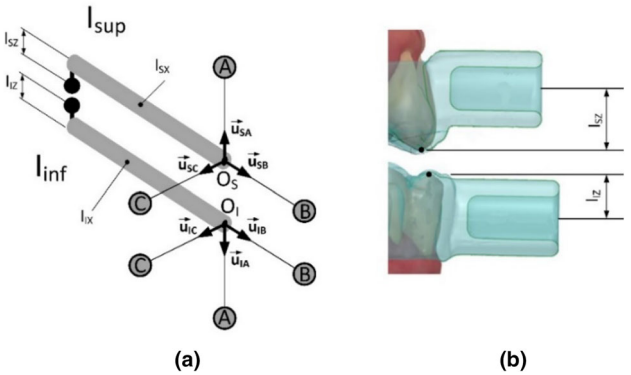

Fig. 3 Upper and lower trihedrons joined, respectively, to the upper and lower incisors. **a** Trihedron model. **b** Detail of the joining between the splints and the incisors

$$\overline{u}_{SB} \times \overline{u}_{SA} = \overline{u}_{SC}, \tag{1}$$

$$\overline{u}_{IA} \times \overline{u}_{IB} = \overline{u}_{IC}, \tag{2}$$

where

$$\begin{cases} \overline{u}_{SA} = \dfrac{1}{l_T} \cdot \begin{bmatrix} x_{SA} - x_{OS} \\ y_{SA} - y_{OS} \\ z_{SA} - z_{OS} \end{bmatrix}, \\ \overline{u}_{SB} = \dfrac{1}{l_T} \cdot \begin{bmatrix} x_{SB} - x_{OS} \\ y_{SB} - y_{OS} \\ z_{SB} - z_{OS} \end{bmatrix}, \\ \overline{u}_{SC} = \dfrac{1}{l_T} \cdot \begin{bmatrix} x_{SC} - x_{OS} \\ y_{SC} - y_{OS} \\ z_{SC} - z_{OS} \end{bmatrix}, \end{cases} \tag{3}$$

$$\begin{cases} \overline{u}_{IA} = \dfrac{1}{l_T} \cdot \begin{bmatrix} x_{IA} - x_{OI} \\ y_{IA} - y_{OI} \\ z_{IA} - z_{OI} \end{bmatrix}, \\ \overline{u}_{IB} = \dfrac{1}{l_T} \cdot \begin{bmatrix} x_{IB} - x_{OI} \\ y_{IB} - y_{OI} \\ z_{IB} - z_{OI} \end{bmatrix}, \\ \overline{u}_{IC} = \dfrac{1}{l_T} \cdot \begin{bmatrix} x_{IC} - x_{OI} \\ y_{IC} - y_{OI} \\ z_{IC} - z_{OI} \end{bmatrix}, \end{cases} \tag{4}$$

where l_T is the distance between the origin of the coordinate system and the markers of each trihedron. From the positions of reference points A, [(x_{IA},y_{IA},z_{IA}), (x_{SA}, y_{SA}, z_{SA})], B, [(x_{IB},y_{IB},z_{IB}), (x_{SB}, y_{SB}, z_{SB})] and C, [(x_{IC},y_{IC},z_{IC}), (x_{SC}, y_{SC}, z_{SC})], the coordinates of points O_I (x_{OI},y_{OI},z_{OI}) and O_S (x_{OS},y_{OS},z_{OS}) can be obtained using Eqs. (1) and (2).Once the locations of the trihedron origins are known, the coordinates of the upper and lower incisors (I_{inf}, I_{sup}) in the global reference system can be calculated from Eqs. (5) and (6):

$$I^0_{\text{inf}} = \begin{bmatrix} x_{I_i} \\ y_{I_i} \\ z_{I_i} \end{bmatrix}^0 = \begin{bmatrix} x_{OI} \\ y_{OI} \\ z_{OI} \end{bmatrix} - l_{IX} \cdot \begin{bmatrix} u^x_{IB} \\ u^y_{IB} \\ u^z_{IB} \end{bmatrix} - l_{IZ} \cdot \begin{bmatrix} u^x_{IA} \\ u^y_{IA} \\ u^z_{IA} \end{bmatrix}, \tag{5}$$

$$I^0_{\text{sup}} = \begin{bmatrix} x_{I_s} \\ y_{I_s} \\ z_{I_s} \end{bmatrix}^0 = \begin{bmatrix} x_{OS} \\ y_{OS} \\ z_{OS} \end{bmatrix} - l_{SX} \cdot \begin{bmatrix} u^x_{SB} \\ u^y_{SB} \\ u^z_{SB} \end{bmatrix} - l_{SZ} \cdot \begin{bmatrix} u^x_{SA} \\ u^y_{SA} \\ u^z_{SA} \end{bmatrix}, \tag{6}$$

where distances l_{IX}, l_{SX}, l_{IZ}, y l_{SZ} are defined in Fig. 3. Next, the model shown in Fig. 5 is used to obtain the movement of the condyles.

In this model, the coordinates of the lower incisor in the reference system linked to the upper incisor $I^S_{\text{inf}} = \{x_{I_i}, y_{I_i}, z_{I_i}\}$ and the unit vectors $\vec{w}$ and $\vec{u}$, parallel to the trihedron vectors $\vec{u}_{IB}$ and $\vec{u}_{IC}$, respectively, are known. Angles

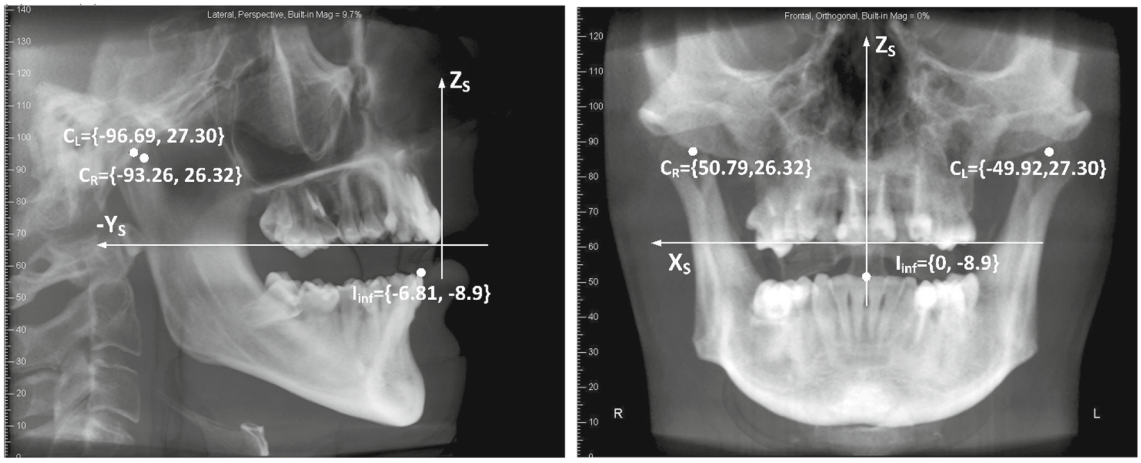

Fig. 4 Lateral and frontal X-ray of the patient with coordinates of the points of interest

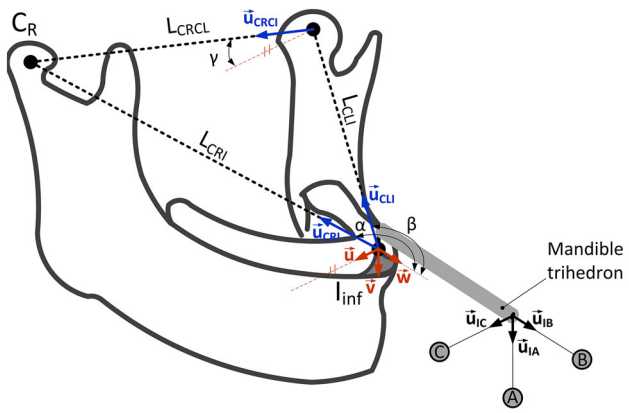

Fig. 5 Model of the jaw to obtain coordinates of the condyle

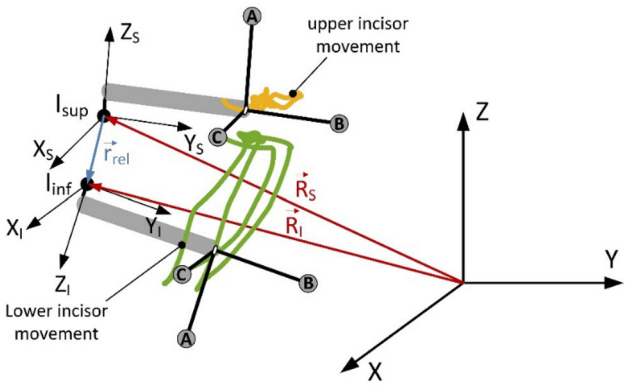

Fig. 6 Upper and lower incisive movement with respect to the absolute reference frame

α, β and γ and distances L_{CRI}, L_{CLI} and L_{CRCL} are also known, since these values can be obtained using the markers located in the condyle or using a frontal and lateral X-ray oriented in the $\vec{w}$ and $\vec{u}$ direction, respectively, as explained before. Therefore, the coordinates of the movement of the lower incisor are (see Fig. 6):

$$\vec{R}_I^0 = \vec{R}_S^0 + \vec{r}_{\mathrm{rel}}^0, \tag{7}$$

$$\vec{r}_{\mathrm{rel}}^0 = \vec{R}_I^0 - \vec{R}_S^0 = \begin{bmatrix} x_{I_i} \\ y_{I_i} \\ z_{I_i} \end{bmatrix}^0 - \begin{bmatrix} x_{I_s} \\ y_{I_s} \\ z_{I_s} \end{bmatrix}^0, \tag{8}$$

$$I_{\mathrm{inf}}^S = \begin{bmatrix} x_{I_i} \\ y_{I_i} \\ z_{I_i} \end{bmatrix} = \vec{r}_{\mathrm{rel}}^S = S^{S0} \cdot \vec{r}_{\mathrm{rel}}^0 \rightarrow S^{S0} = \begin{bmatrix} u_{SC}^x & u_{SC}^y & u_{SC}^z \\ u_{SB}^x & u_{SB}^y & u_{SB}^z \\ u_{SA}^x & u_{SA}^y & u_{SA}^z \end{bmatrix}. \tag{9}$$

Once these data have been obtained, the following equations provide the position of the condyles with respect to the reference point of the lower incisor:

$$\left(x_{\mathrm{CR}} - x_{I_i}\right)^2 + \left(y_{\mathrm{CR}} - y_{I_i}\right)^2 + \left(z_{\mathrm{CR}} - z_{I_i}\right)^2 - L_{\mathrm{CRI}}^2 = 0, \tag{10}$$

$$\left(x_{\mathrm{CL}} - x_{I_i}\right)^2 + \left(y_{\mathrm{CL}} - y_{I_i}\right)^2 + \left(z_{\mathrm{CL}} - z_{I_i}\right)^2 - L_{\mathrm{CLI}}^2 = 0, \tag{11}$$

$$(x_{\mathrm{CR}} - x_{\mathrm{CL}})^2 + (y_{\mathrm{CR}} - y_{\mathrm{CL}})^2 + (z_{\mathrm{CR}} - z_{\mathrm{CL}})^2 - L_{\mathrm{CRCL}}^2 = 0, \tag{12}$$

$$\left(x_{I_i} - x_{\mathrm{CR}}\right) \cdot w_x + \left(y_{I_i} - y_{\mathrm{CR}}\right) \cdot w_y + \left(z_{I_i} - z_{\mathrm{CR}}\right) \cdot w_z - L_{\mathrm{CRI}} \cdot \cos\alpha = 0, \tag{13}$$

$$\left(x_{I_i} - x_{\mathrm{CL}}\right) \cdot w_x + \left(y_{I_i} - y_{\mathrm{CL}}\right) \cdot w_y + \left(z_{I_i} - z_{\mathrm{CL}}\right) \cdot w_z - L_{\mathrm{CLI}} \cdot \cos\beta = 0, \tag{14}$$

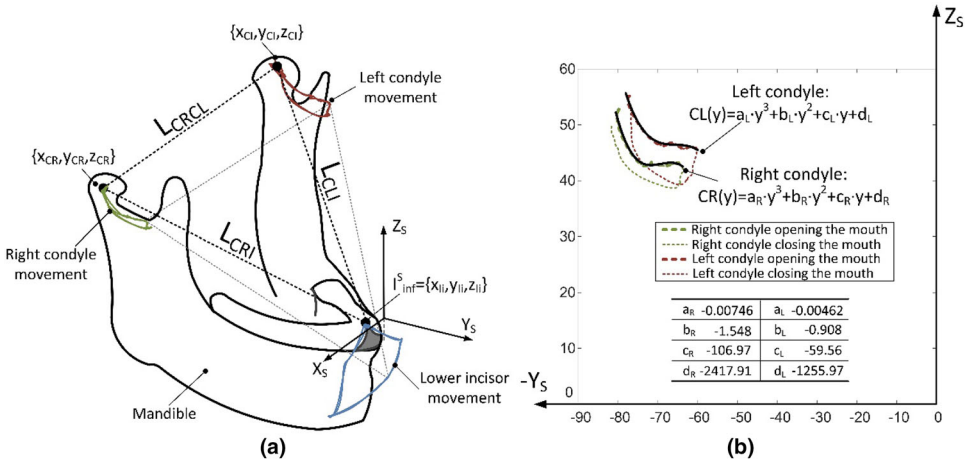

Fig. 7 Condyle movements. **a** 3D model. **b** Adjustment of condyle curves in the sagittal plane

Table 1 Patient's biometric values

L_{CRI} (mm)	L_{CLI} (mm)	L_{CRCL} (mm)	α (°)	β (°)	γ (°)
106.27	109	100.77	144.44	145.62	2.18

$$(y_{CR} - y_{CL}) \cdot u_z - (z_{CR} - z_{CL}) \cdot u_y - u_x \cdot L_{CRCI} \cdot \sin\gamma = 0, \tag{15}$$

$$(z_{CR} - z_{CL}) \cdot u_x - (x_{CR} - x_{CL}) \cdot u_z - u_y \cdot L_{CRCI} \cdot \sin\gamma = 0, \tag{16}$$

$$(x_{CR} - x_{CL}) \cdot u_y - (y_{CR} - y_{CL}) \cdot u_x - u_z \cdot L_{CRCI} \cdot \sin\gamma = 0. \tag{17}$$

The coordinates of the condyles $C_R = \{x_{CR}, y_{CR}, z_{CR}\}$ and $C_I = \{x_{CI}, y_{CI}, z_{CI}\}$ are calculated from the previous set of equations, Eqs. (10) to (17). Note that the coordinates of the position of the lower incisor used in the equations are not referred to the global system [Eq. (5)] but to the coordinate system linked to the upper incisor. This way, it is possible to determine the movement of the jaw with respect to the maxilla even when the latter is moving (see Fig. 6).

Once the coordinates of the position of the condyle with respect to the reference system linked to the upper incisor have been obtained, two third-order polynomial curves are fitted to reproduce the trajectory of the left and right condyles, respectively (see Fig. 7). These curves (see Fig. 7b) are obtained using the patient's data shown in Table 1. It can be seen that the trajectories followed by the right and left condyles are different. While the use of a 2D jaw model performs well in many cases, the use of the proposed 3D model allows obtaining a more precise description of the movement of both condyles. As it is shown in Fig. 7b, only the trajectory of the condyle during the mouth opening and protrusion movements in Posselt's diagram has been fitted. These curves are used to design a customized MAD in the next section.

Design of a mandibular advancement device

Three points are defined to model the solid that reproduces the jaw. These three points are located in the condyles and in the lower incisor (see Fig. 8). The reference axes are defined with the origin of the coordinate system located on the upper incisor that remains fixed to the skull. Therefore, the set of natural coordinates [27] are:

$$q = \left\{x_{CR}, y_{CR}, z_{CR}, x_{CL}, y_{CL}, z_{CL}, x_{I_i}, y_{I_i}, z_{I_i}\right\}. \tag{18}$$

The joint of the condyle with the mandibular fossa is a kinematic pair with 5 degrees of freedom (DOF). The movement of the condyle in a perpendicular direction to the fossa shape, due to the deformation of the joint disk, is considered negligible. Therefore, the mandible model has 4 DOF. Thus, the coordinate set is not free and 5 restriction equations are introduced:

$$\left(x_{CR} - x_{I_i}\right)^2 + \left(y_{CR} - y_{I_i}\right)^2 + \left(z_{CR} - z_{I_i}\right)^2 - L_{CRI}^2 = 0, \tag{19}$$

$$\left(x_{CL} - x_{I_i}\right)^2 + \left(y_{CL} - y_{I_i}\right)^2 + \left(z_{CL} - z_{I_i}\right)^2 - L_{CLI}^2 = 0, \tag{20}$$

$$(x_{CR} - x_{CL})^2 + (y_{CR} - y_{CL})^2 + (z_{CR} - z_{CL})^2 - L_{CRCL}^2 = 0, \tag{21}$$

$$z_{CR} - \left(a_R \cdot y_{CR}^3 + b_R \cdot y_{CR}^2 + c_R \cdot y_{CR} + d_R\right) = 0, \tag{22}$$

$$z_{CL} - \left(a_L \cdot y_{CL}^3 + b_L \cdot y_{CL}^2 + c_L \cdot y_{CL} + d_L\right) = 0. \tag{23}$$

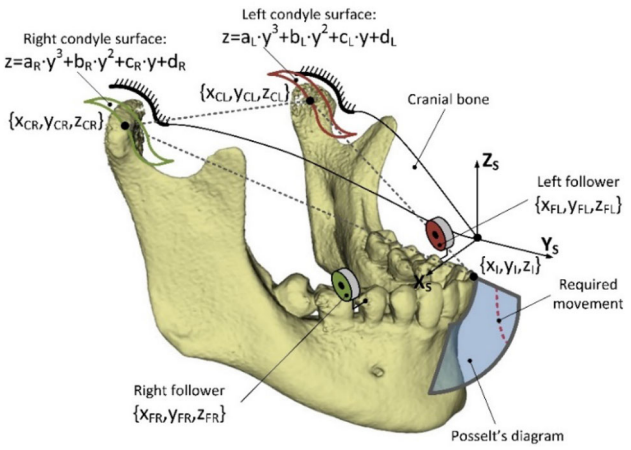

Fig. 8 Multibody model of the mandible

Equations (19) to (21) define the rigid solid condition of points CR, CL and I. Equations (22) and (23) set the condition for the movement of the condyles in the curves defined by the glenoid fossas. These curves were calculated in the previous section. Thus, the condyles can move on a surface where the y_{CR} and z_{CR} coordinates of the right condyle and the y_{CL} and z_{CL} coordinates of the left condyle change according to Eqs. (22) and (23). In the case of the x_{CR} and x_{CL} coordinates, these are established by the restrictions in our model and the movement of the jaw. Therefore, a surface parallel to the Y_S Z_S plane is defined for the movement of the condyles (see Fig. 8).

In order to reproduce the mandibular movement when a patient uses the MAD, 4 restrictions for the 4 DOF of the jaw are introduced. In this paper, the following data are used:

- The positions of the lower incisor $I_{\text{inf}}^S = \{x_{I_i}, y_{I_i}, z_{I_i}\}$ for the correct functioning of the device when patients' open their mouth. These positions are points on the desired trajectory for the lower incisor prescribed by the specialist to ensure that the jaw is kept in a protruded position. In the example developed in this paper 9 positions have been used.
- The coordinate $\{x_{CR}\}$ of the right condyle. This restricts the lateral movement of the jaw when designing the device cams. However, this movement will be allowed in the final design of the device, allowing patients to move their jaw laterally as we will see later.

An iterative process is proposed to solve the kinematics of the model in Eq. (24):

$$\Phi_q(\boldsymbol{q}) \cdot \left(\boldsymbol{q}_{i+1} - \boldsymbol{q}_i\right) = -\Phi(\boldsymbol{q}), \tag{24}$$

where $\boldsymbol{q}$ is the set of natural coordinates defined in (18), $\Phi(\boldsymbol{q})$ is the set of constraints defined in Eqs. (19) to (23) and $\Phi_q(\boldsymbol{q})$ is the Jacobian of the set of constraints with respect to the coordinates. Once the system (24) has been solved for all input positions, the movement of any point on the jaw can be obtained.

If the position of any singular point during jaw movement has to be known, the generalized set of coordinates has to be increased with the coordinates of that point [Eq. (25)]. This is used to know the positions of two followers of the cams of the device (see Fig. 8).

$$q = \left\{ \begin{matrix} x_{CR}, y_{CR}, z_{CR}, x_{CL}, y_{CL}, z_{CL}, x_{I_i}, y_{I_i}, z_{I_i}, x_{FR}, y_{FR}, z_{FR}, \\ x_{FL}, y_{FL}, z_{FL} \end{matrix} \right\}, \tag{25}$$

$$\left(x_{FR} - x_{I_i}\right) - \alpha_{FR} \cdot \left(x_{CR} - x_{I_i}\right) - \beta_{FR} \cdot \left(x_{CL} - x_{I_i}\right) - \gamma_{FR} \cdot (x_{CR} - x_{CL}) = 0, \tag{26}$$

$$\left(y_{FR} - y_{I_i}\right) - \alpha_{FR} \cdot \left(y_{CR} - y_{I_i}\right) - \beta_{FR} \cdot \left(y_{CL} - y_{I_i}\right) - \gamma_{FR} \cdot (y_{CR} - y_{CL}) = 0, \tag{27}$$

$$\left(z_{FR} - z_{I_i}\right) - \alpha_{FR} \cdot \left(z_{CR} - z_{I_i}\right) - \beta_{FR} \cdot \left(z_{CL} - z_{I_i}\right) - \gamma_{FR} \cdot (z_{CR} - z_{CL}) = 0, \tag{28}$$

$$\left(x_{FL} - x_{I_i}\right) - \alpha_{FL} \cdot \left(x_{CR} - x_{I_i}\right) - \beta_{FL} \cdot \left(x_{CL} - x_{I_i}\right) - \gamma_{FL} \cdot (x_{CR} - x_{CL}) = 0, \tag{29}$$

$$\left(y_{FL} - y_{I_i}\right) - \alpha_{FL} \cdot \left(y_{CR} - y_{I_i}\right) - \beta_{FL} \cdot \left(y_{CL} - y_{I_i}\right) - \gamma_{FL} \cdot (y_{CR} - y_{CL}) = 0, \tag{30}$$

$$\left(z_{FL} - z_{I_i}\right) + \alpha_{FL} \cdot \left(z_{CR} - z_{I_i}\right) - \beta_{FL} \cdot \left(z_{CL} - z_{I_i}\right) - \gamma_{FR} \cdot (z_{CR} - z_{CL}) = 0. \tag{31}$$

Using Eqs. (19) to (23) and (26) to (31), the movements of the centre of each follower are obtained and, consequently, the path they have to follow to ensure that the lower incisor moves along the trajectory established by the specialist to guarantee of the MAD.

Equations (26) to (31) provide the points of the right and left follower with respect to the base formed by points C_R, C_L and I_{inf}. Parameters α_{FR}, β_{FR}, γ_{FR}, α_{FL}, β_{FL}, and γ_{FL} are determined by the position that the designer determines to be appropriate for the followers.

Figure 9 shows the mandible movement sequence of a patient whose data are given in Table 1 (see Online Resource 1). The data for the position of the followers and the coefficients of the condyle curves for this example are exposed

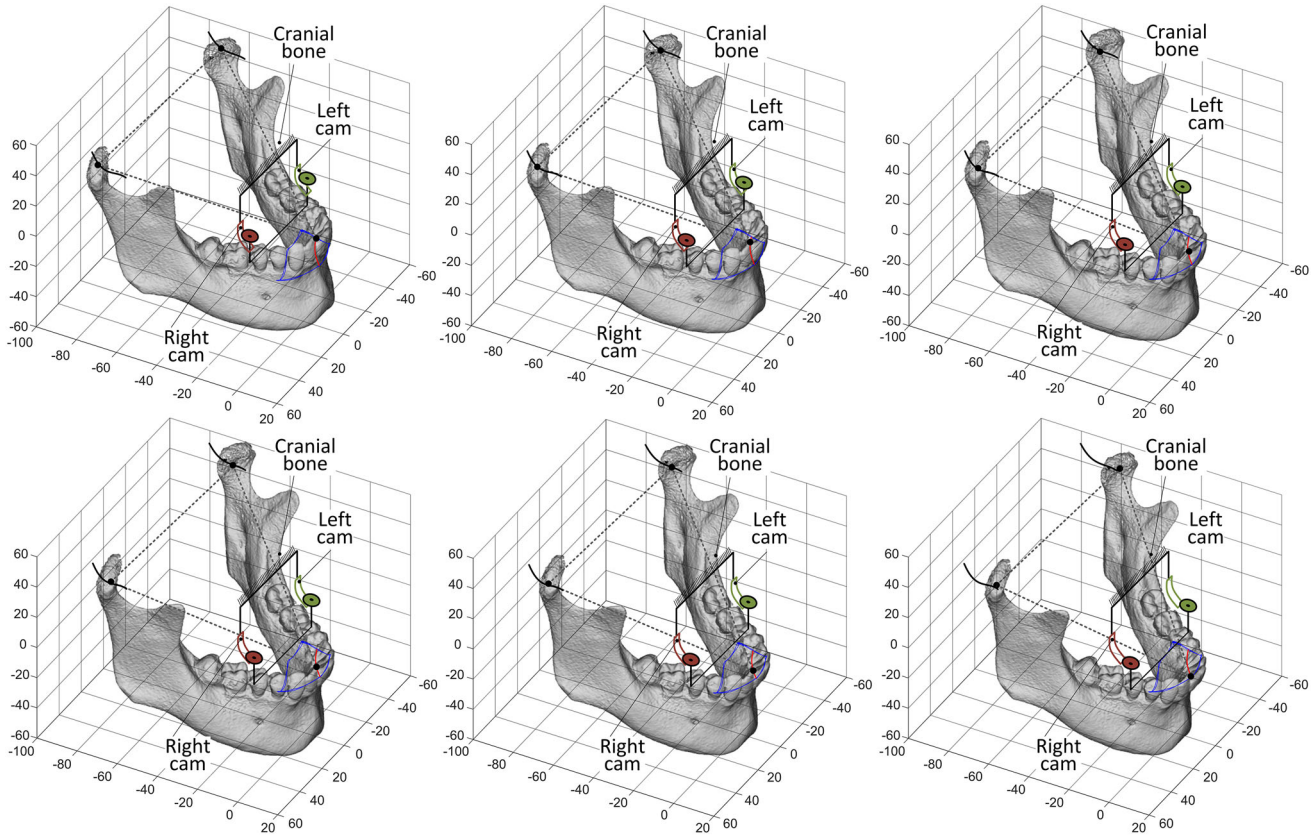

Fig. 9 Mandible movement sequence with cams and followers

Table 2 Parameters to obtain the position of the followers and the condyle curves

α_{FR}	β_{FR}	γ_{FR}	a_R	b_R	c_R	d_R
− 90.0778	90.3106	90.3660	− 0.00746	− 1.548	− 106.97	− 2417.91
α_{FL}	β_{FL}	γ_{FL}	a_L	b_L	c_L	d_L
− 17.2905	17.5261	17.2628	− 0.00462	− 0.908	− 59.56	− 1255.97

Table 3 *X*, *Y* and *Z* coordinates of the condyles and lower incisor

	x (mm)	*y* (mm)	*z* (mm)		*x* (mm)	*y* (mm)	*z* (mm)		*x* (mm)	*y* (mm)	*z* (mm)
I_{i1}	1.36	5.97	− 3.14	C_{R1}	44.86	− 76.66	45.13	C_{L1}	− 55.80	− 73.25	48.73
I_{i2}	− 1.30	5.65	− 5.55	C_{R2}	44.86	− 75.98	44.44	C_{L2}	− 55.79	− 72.37	48.06
I_{i3}	− 1.24	5.45	− 7.69	C_{R3}	44.86	− 75.24	43.86	C_{L3}	− 55.78	− 71.42	47.50
I_{i4}	− 1.19	5.38	− 9.65	C_{R4}	44.86	− 74.38	43.37	C_{L4}	− 55.77	− 70.35	47.05
I_{i5}	− 1.13	5.46	− 11.53	C_{R5}	44.86	− 73.31	43.00	C_{L5}	− 55.76	− 69.06	46.71
I_{i6}	− 1.07	5.71	− 13.43	C_{R6}	44.86	− 71.88	42.81	C_{L6}	− 55.75	− 67.42	46.50
I_{i7}	− 1.01	6.16	− 15.43	C_{R7}	44.86	− 69.88	42.94	C_{L7}	− 55.76	− 65.31	46.41
I_{i8}	− 0.96	6.82	− 17.63	C_{R8}	44.86	− 67.27	43.24	C_{L8}	− 55.78	− 62.78	46.25
I_{i9}	− 0.90	7.72	− 20.13	C_{R9}	44.86	− 64.57	42.92	C_{L9}	− 55.79	− 60.14	45.54

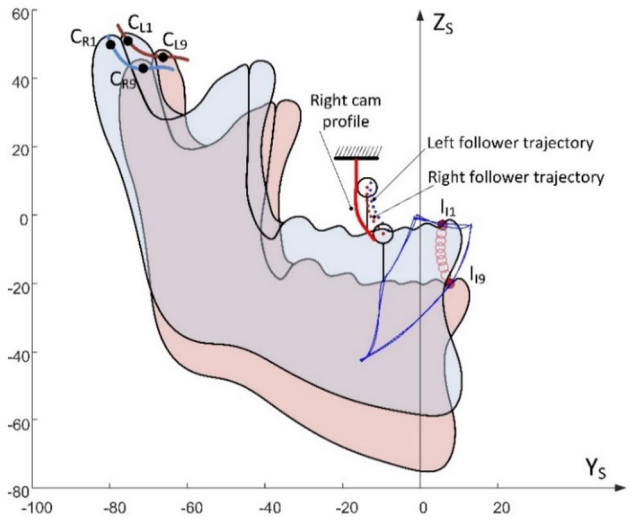

Fig. 10 Profile of the right cam linked to the maxilla

Table 4 *X*, *Y* and *Z* coordinates of the centre of the followers

	x (mm)	*y* (mm)	*z* (mm)		*x* (mm)	*y* (mm)	*z* (mm)
F_{R1}	14.97	− 13.46	7.90	F_{L1}	− 16.97	− 12.61	9.18
F_{R2}	15.02	− 13.56	5.90	F_{L2}	− 16.92	− 12.63	7.19
F_{R3}	15.06	− 13.55	4.12	F_{L3}	− 16.88	− 12.56	5.42
F_{R4}	15.10	− 13.42	2.49	F_{L4}	− 16.83	− 12.36	3.82
F_{R5}	15.15	− 13.12	0.96	F_{L5}	− 16.79	− 11.98	2.30
F_{R6}	15.19	− 12.60	− 0.54	F_{L6}	− 16.74	− 11.40	0.80
F_{R7}	15.23	− 11.80	− 2.03	F_{L7}	− 16.70	− 10.56	− 0.76
F_{R8}	15.28	− 10.68	− 3.62	F_{L8}	− 16.66	− 9.46	− 2.50
F_{R9}	15.32	− 9.36	− 5.59	F_{L9}	− 16.62	− 8.15	− 4.60

in Table 2. As shown in Fig. 9, the cams are attached to the maxilla and the followers to the mandible in this example. This is done by means of two splints with the dental impression of the patient. The trajectories of the condyles when the lower incisor follows the nine prescribed positions are shown in Table 3.

The trajectories of the centre of the followers in the sagittal plane ($y_{FR}, z_{FR}, y_{FL}, z_{FL}$) are determined to design the profile of the cams, as mentioned above. Knowing the radius of the followers, the cam profiles are determined by finding the contact points in each position between the cam and the follower (see Fig. 10) [25].

For the sake of clarity, only the profile of the right cam has been drawn in Fig. 10. However, it has to be emphasized that the trajectories of the centre of the followers are not symmetrical with respect to the sagittal plane (see Table 4). Therefore, the position of the left cam can be different from the right one in the sagittal plane.

The methodology proposed in this paper has been compared to the methodology described in the previous work [25]. To this end, two MADs have been designed. The first MAD has been obtained using the measurement system and 3D jaw model described in this paper. Next, a second MAD has been designed using the previous methodology. Figure 11 shows the result of this comparison. It can be seen that the trajectory followed by the lower incisor with the new approach allows a wider mouth opening (19.7 mm) compared to the one obtained with the previous method (11.8 mm). As expected, the cam profile obtained with the previous methodology yields to a lower incisor movement being restricted to the sagittal plane. On the contrary, the new device allows a 3D movement of the lower incisor. As we can see in Fig. 11, if the specialist prescribes a MAD able to provide a vertical opening of the mouth of 17 mm, the trajectory followed by the lower incisor in the 3D case is correct and the advancement when the patient opens the mouth is always positive (Fig. 11b). However, the advancement is negative and the device loses effectiveness when using the device designed with the 2D model.

As it has been shown, the methodology proposed in this paper can cope with irregularities in the temporomandibular joints and in the trajectory followed by the condyles. Personalized MAD's obtained with this approach have better performance compared to previous methodologies since the cam profiles in the designed devices allow a wider range of mouth opening. Thus, this methodology allows designing devices for patients with asymmetries in the jaw movement.

The result of the comparison of devices obtained with 2D and 3D models suggests that the use of a 3D model will lead to designing better fitted cam devices according to patients' requirements. However, this comparison has been conducted with only one patient. This claim should be validated with tests on a wider range of patients to confirm the benefits of the proposed methodology.

In the model developed above, the cam is fixed to the maxilla and the follower moves with the mandible. However, when the cam is attached to the mandible and the follower fixed to the maxilla, the same relative motion is obtained [25]. The latter is the configuration used in the device shown in Fig. 12. It can also be seen that there is a lateral space between the upper splint and the cams, which allows lateral movement of the jaw.

The final device (Fig. 12b) was printed in a Formiga P 110 Velocis by EOS GmbH (Germany) 3D printer using selective laser sintering technology (SLS). A biocompatible material, Polyamide 12 powder with trade name PA2200, manufactured by EOS GmbH, was used. This way, an accurate position of the cams and followers, ensuring the correct functioning of the device and contributing to a perfect fit in the patient's dental arches, was achieved.

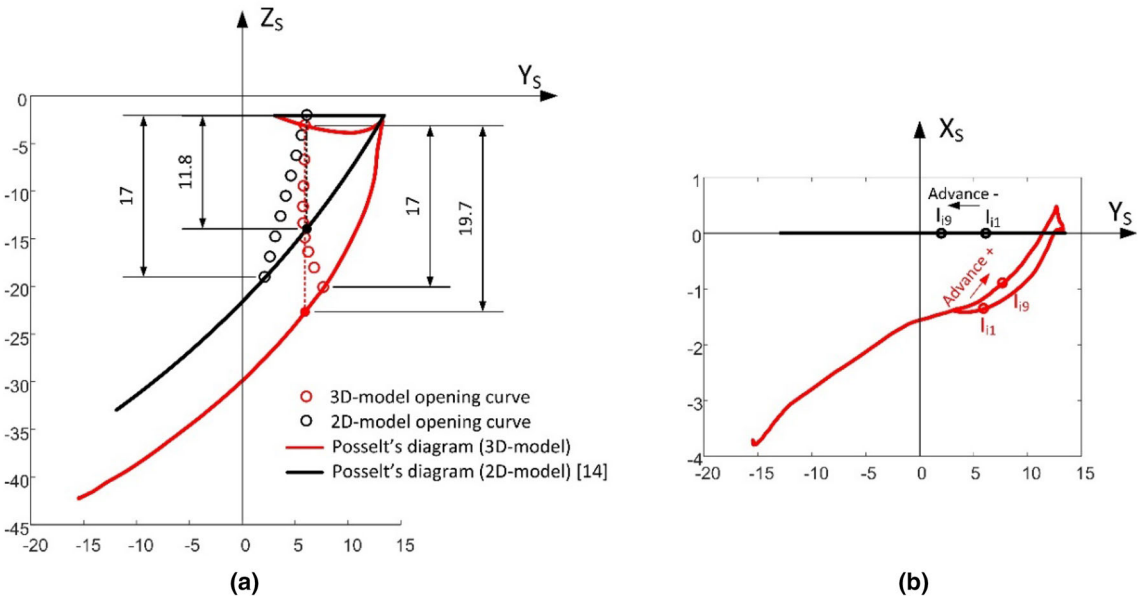

Fig. 11 3D-model versus 2D-model comparative study. **a** Posselt's diagrams in the sagittal plane. **b** Posselt's diagrams in the horizontal plane

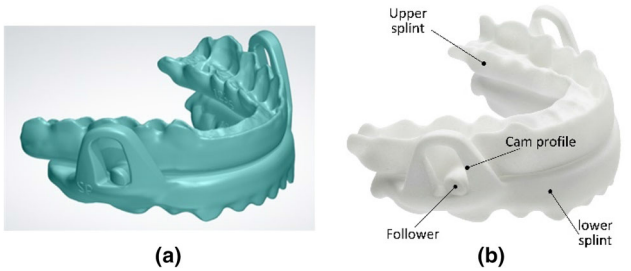

Fig. 12 Final design of MAD. **a** CAD/CAM model device. **b** Real device printed in 3D®

Final considerations

This paper presents a methodology to accurately obtain and reproduce the 3D movement of the jaw in order to design customized MADs. The use of 2D jaw models performs well in many cases. However, the proposed 3D model yields to a more accurate description of the movement of both condyles. Consequently, it is possible to take into account asymmetries or malformations in the temporomandibular joints in the design stage of MADs.

This way, a 3D multibody model that reproduces the jaw movement has been described in this work. The movement of the human jaw has been studied and the appropriate movement restrictions of the jaw in the temporomandibular joint have been defined to obtain the 3D model. Thus, the movement of the lower incisor has been obtained by means of a vision system based on the use of infrared cameras and reflective markers. These data have made it possible to obtain the movement of the condyles.

Once the 3D model is developed, the movement of the jaw can be obtained when using a MAD. To this end, the desired trajectory of the lower incisor has to be previously defined. This trajectory is prescribed by a specialist to ensure the appropriate mandible advancement throughout its opening movement. This way, it is possible to accurately model the movement of the jaw and therefore obtain the trajectory of any other point attached to the mandible, such as the two followers of the MAD. Finally, the trajectories of the followers determine the design of the cams.

The development of a 3D model of the mandible makes it possible to obtain a more precise profile of the cam and its positioning in the splint. This is important since most patients do not have symmetrical jaws with respect to the sagittal plane. Therefore, a 3D study of the movement is necessary to ensure that the movement of the patient's jaw is natural and comfortable when using the device even if the patient suffers from problems in the temporomandibular joints. With this work, these problems can be detected and the design of the mandibular advancement device can be properly addressed. However, further works will be devoted to the study of MADs specifically designed for patients who suffer from serious problems in the temporomandibular joints in which specialists report poor performance of current devices. In addition, the comparison between cam designs obtained using 2D and 3D models will be conducted with a wider

sample of patients to confirm the claimed advantages of the use of a 3D model in the design of cams.

Acknowledgements A substantial part of the work described in this article was supported by the research Contracts 806/31.4830 and 806/31.5511 between the private company Laboratorio Ortoplus S.L. and the University of Málaga, which is acknowledged with gratefulness.

Author contributions Conceptualization and methodology, MG, JAC and AB; Investigation, all authors; Writing-original draft; JAC, AB and JJC; Writing-review and editing, all authors.

Compliance with ethical standards

Conflict of interest M. García, J.A. Cabrera, A. Bataller, S. Postigo and J.J. Castillo declare that they have no conflict of interest.

Ethical approval This study does not contain any studies with human or animal subjects performed by any of the authors.

References

1. Dempsey JA, Veasey SC, Morgan BJ, O'Donnell CP (2010) Pathophysiology of sleep apnea. Phys Rev 90(1):47–112. https://doi.org/10.1152/physrev.00043.2008
2. Malhotra A, White DP (2002) Obstructive sleep apnoea. Lancet 360(20):238–245
3. Douglas Bradley T, Floras JS (2009) Obstructive sleep apnoea and its cardiovascular consequences. Lancet 373(3):82–93
4. Wang H, Newton JD, Floras JS, Mak S, Chiu K-L, Ruttanaumpawan P, Tomlinson G, Douglas Bradley T (2007) Influence of obstructive sleep apnea on mortality in patients with heart failure. J Am Coll Cardiol 49(15):1. https://doi.org/10.1016/j.jacc.2006.12.046
5. Klar Yaggi H, Concato J, Kernan WN, Lichtman JH, Brass LM, Mohsenin V (2005) Obstructive sleep apnea as a risk factor for stroke and death. N Engl J Med 353(10):2034–2041
6. Epstein LJ, Kristo D, Strollo J Jr, Friedman N, Malhotra A, Patil SP, Ramar K, Rogers R, Schwab RJ, Weaver EM, Weinstein MD (2009) Clinical guideline for the evaluation, management and long-term care of obstructive sleep apnea in adults. J Clin Sleep Med 5(3):263–276
7. Sutherland K, Vanderveken OV, Tsuda H, Marklund M, Gagnadoux F, Kushida CA, Cistulli PA (2014) Oral appliance treatment for obstructive sleep apnea: an update. J Clin Sleep Med 10:215–227
8. Lloberes P, Durán-Cantolla J, Martínez-García MA, Marín JM, Ferrer A, Corral J, Masa JF, Parra O, Alonso-Alvárez ML, Terán-Santos J (2011a) Diagnóstico y tratamiento del síndrome de apneas-hipopneas del sueño. Arch Bronconeumol. https://doi.org/10.1016/j.arbres.2011.01.001
9. Lloberes P, Durán-Cantolla J, Martínez-García MA, Marín JM, Ferrer A, Corral J, Masa JF, Parra O, Alonso-Alvárez ML, Terán-Santos J (2011b) Fe de errores de 'Diagnóstico y tratamiento del síndrome de apneas-hipopneas del sueño'. Arch Bronconeumol. https://doi.org/10.1016/j.arbres.2011.04.001
10. Bhat W, Jayesh S (2015) Mandibular advancement device for obstructive sleep apnea: an overview. J Pharm Bioallied Sci 7:s223–s225. https://doi.org/10.4103/0975-7406.155915
11. Sutherland K, Takaya H, Qian J, Petocz P, Andrew T, Cistulli PA (2015) Oral appliance treatment response and polysomnographic phenotypes of obstructive sleep apnea. J Clin Sleep Med 11:861–868
12. Sutherland K, Cistullia PA (2011) Mandibular advancement splints for the treatment of sleep apnea syndrome. Swiss Med Wkly 141(September):w13276. https://doi.org/10.4414/smw.2011.13276
13. Dieltjens M, Vanderveken OM, Van de Heyning PH, Braem MJ (2012) Current opinions and clinical practice in the titration of oral appliances in the treatment of sleep-disordered breathing. Sleep Med Rev 16:177–185. https://doi.org/10.1016/j.smrv.2011.06.002
14. Xu WL, Bronlund JE, Potgieter J, Foster KD, Röhrle O, Pullan AJ, Kieser JA (2008) Review of a human masticatory system and masticatory robotics. Mech Mach Theory 43:1353–1375
15. Daumas B, Xu L, Bronlund J (2005) Jaw mechanism modeling and simulation. Mech Mach Theory 40:821–833
16. Takanobu H, Takanishi A, Ozawa D, Ohtsuki K, Ohnishi M, Okino A (2002) Integrated dental robot system for mouth opening and closing training. In: Proceeding of the 2002 IEEE international conference on robotics and automation, pp 1428–1433
17. Lee SJ, Kim BK, Chun YG, Park DJ (2018) Design of mastication robot with life-sized linear actuator of human muscle and load cells for measuring force distribution on teeth. Mechatronics 51:127–136
18. Xu WL, Pap JS, Bronlund J (2008) Design of a biologically inspired parallel robot for foods chewing. IEEE Trans Ind Electron 55:832–841
19. Delsignore MJ, Krovi VN (2008) Screw-theoretic analysis models for felid jaw mechanisms. Mech Mach Theory 43:147–159
20. Posselt U (1952) Studies in the mobility of the human mandible. Acta Scand 10:1–60
21. Yuan F, Sui H, Li Z, Yang H, Lü P, Wang Y, Sun Y (2015) A method of three-dimensional recording of mandibular movement based on two-dimensional image feature extraction. PLoS ONE 10(9):e0137507. https://doi.org/10.1371/journal.pone.0137507
22. Fang JJ, Kuo TH (2008) Modelling of mandibular movement. Comput Biol Med 38:1152–1162
23. Enciso R, Memon A, Fidaleo DA, Neumann U, Mah J (2003) The virtual craniofacial patient: 3D jaw modeling and animation. Stud Health Technol Inform 94:65–71
24. Pinheiro AP, Pereira AA, Andrade AO, Bellomo D (2011) Measurement of jaw motion: the proposal of a simple and accurate method. J Med Eng Techonol 35:125–133
25. Bataller A, Cabrera JA, García M, Castillo JJ, Mayoral P (2018) Cam synthesis applied to the design of a customized mandibular advancement device for the treatment of obstructive sleep apnea. Mech Mach Theory 123:153–165
26. Reyes M, Sanz PM, Guerrero AF (2017) Determining the mandibular normal range of motions in young adults: a guide for diagnosis and treatment of patients with mandibular advance devices. Sleep Med 40:185
27. García de Jalón J, Bayo E (1994) Kinematic and dynamic simulation of multibody systems. Springer, New York